Published in final edited form as:
Pflugers Arch. 2010 August ; 460(3): 633–644. doi:10.1007/s00424-010-0842-0.

Control of Volume-Sensitive Chloride Channel Inactivation by the Coupled Action of Intracellular Chloride and Extracellular Protons

Carmen Y. Hernández-Carballo[1], **José A. De Santiago-Castillo**[2], **Teresa Rosales-Saavedra**[2], **Patricia Pérez-Cornejo**[2], and **Jorge Arreola**[1]

[1] Instituto de Física, Universidad Autónoma de San Luis Potosí Ave. Dr. Manuel Nava #6, San Luis Potosí, SLP 78290, México

[2] Facultad de Medicina, Universidad Autónoma de San Luis Potosí Ave. Venustiano Carranza # 2405, San Luis Potosí, SLP 78290, México

Abstract

The volume-sensitive chloride current (I_{ClVol}) exhibit a time-dependent decay presumably due to channel inactivation. In this work, we studied the effects of Cl^- and H^+ ions on I_{ClVol} decay recorded in HEK-293 and HL-60 cells using the whole-cell patch clamp technique. Under control conditions ($[Cl^-]_e = [Cl^-]_i = 140$ mM and $pH_i = pH_e = 7.3$), I_{ClVol} in HEK cells shows a large decay at positive voltages but in HL-60 cells I_{ClVol} remained constant independently of time. In HEK-293 cells, simultaneously raising the $[Cl^-]_e$ and $[Cl^-]_i$ from 25 to 140 mM (with $pH_e = pH_i = 7.3$) increased the fraction of inactivated channels (FIC). This effect was reproduced by elevating $[Cl^-]_i$ while keeping the $[Cl^-]_e$ constant. Furthermore, a decrease in pH_e from 7.3 to 5.5 accelerated current decay and increased FIC when $[Cl^-]$ was 140 mM but not 25 mM. In HL-60 cells a slight I_{ClVol} decay was seen when the pH_e was reduced from 7.3 to 5.5. Our data show that inactivation of I_{ClVol} can be controlled by changing either the Cl^- or H^+ concentration or both. Based on our results and previously published data we have built a model that explains VRAC inactivation. In the model the H^+ binding site is located outside the electrical field near the extracellular entry whilst the Cl^- binding site is intracellular. The model depicts inactivation as a pore constriction that happens by simultaneous binding of H^+ and Cl^- ions to the channel followed by a voltage-dependent conformational change that ultimately causes inactivation.

Keywords

Volume regulation; Cl^- channels; Inactivation; pH dependence; Chloride

Introduction

In mammalian cells, volume-regulated anion channels (VRAC) serve as an exit pathway for chloride ions (Cl^-) during regulatory volume decrease [9,15,18]. In addition VRAC play a role in physiological processes such as cell proliferation, differentiation and cell migration as well as apoptosis. In patho-physiological processes VRAC is responsible for the acquisition of cisplatin resistance by cancer cells, the death of cardiomyocytes and hippocampal neurons induced by ischaemia–reperfusion and the necrosis of glial and neuronal cells [19].

Corresponding Author: Dr. Jorge Arreola, Instituto de Física, Universidad Autonóma de San Luis Potosí, Dr. Manuel Nava #6, Zona Universitaria, San Luis Potosí, SLP 78290, México, Tel. (444) 826-2363 ext 136, Fax (444) 813-3874, Arreola@dec1.ifisica.uaslp.mx.

The chloride current (I_{ClVol}) generated by activation of intermediate conductance VRAC show little voltage dependence, however, with strong depolarisations I_{ClVol} rapidly decays to nearly zero in BC_3H1 cells [26]. It is thought that such decay is due to a mechanism similar to a classical inactivation process present in voltage gated cation channels [11]. However, in blood cells such as macrophages, lymphocytes and neutrophils, I_{ClVol} is generated by activation of small conductance VRAC and displays almost no decay at any voltage [3,12,18,20,25]. The bases for such differences remain undetermined.

It has been reported that I_{ClVol} decay is subject to regulation by different external ions including, Ca^{2+}, Mg^{2+}, H^+ and permeant anions. For example, increasing concentrations of Ca^{2+}, Mg^{2+} and H^+ in the extracellular media resulted in enhancement of channel inactivation [16,23,26]. Furthermore, lowering $[Cl^-]_e$ accelerates inactivation and decreases the rate of recovery from inactivation whilst replacing extracellular Cl^- with SCN^-, I^- or Br^- decreases the rate of VRAC inactivation in M-1 duct cells [13,26]. The effects of cations on inactivation cannot be explained by invoking an alteration in surface potential since this would cause the inactivation-voltage curve to be shifted towards positive voltages as the cation concentration increase. Yet, it has been demonstrated that a decrease in extracellular pH or increase in Mg^{2+} concentration results in either a negative shift or no change [26]. Interestingly, both cations and anions affect inactivation only at positive voltages. This could be due to a voltage-dependent interaction between the ions and the channel protein; however, in the case of cations this mechanism would require an enormous amount of energy since the cations will have to overcome a positive field in order to interact with the channel inside the membrane electrical field.

Therefore, it seems H^+, Mg^{2+}, and Cl^- ions all affect I_{ClVol} inactivation through different mechanisms. One possibility is that those mechanisms are different because the ions involved bind to distinct sites on the channel. Thus, to understand how H^+ and Cl^- regulate the inactivation process in I_{ClVol} we studied I_{ClVol} decay in two different mammalian cell lines that display distinct degree of inactivation. Our data show that in HEK-293 cells, I_{ClVol} decay is facilitated by external acidification and by an increase in the intracellular $[Cl^-]$. The enhancement of inactivation by acidification of the external media was largely attenuated by decreasing the $[Cl^-]$. In contrast, I_{ClVol} from human promyelocitic HL-60 cells did not show decay in the presence of 140 mM Cl^- even at +120 mV, instead a slight inactivation was induced by external acidification. Our experimental and analytical results indicate that the mechanism of I_{ClVol} decay is not solely voltage-dependent but includes the concerted action of anions and protons.

Material and Methods

Cell Culture

HEK-293H cells obtained from Invitrogen (Carlsbad, CA) were maintained at 37°C in a 95% O_2/5% CO_2 atmosphere in Dulbecco's Modified Eagle Medium (DMEM from GIBCO; Carlsbad, CA), supplemented with 10% Fetal Bovine Serum (FBS), 5.5mM Sodium Piruvate and 500 μl gentamicin (GIBCO; 10 mg/ml). Cells were grown to 80-90% confluence and later detached using 0.1% Trypsin (GIBCO) in a Ca^{2+} and Mg^{2+}-free Hank's balanced salt solution (HBSS 1X from GIBCO). The HBSS contained (in mM): 137.9 NaCl, 5.3 KCl, 0.4 KH_2PO_4, 4.2 $NaHCO_3$, 0.3 Na_2HPO_4, 5.5 D-Glucose and pH= 7.0-7.4. After trypsin treatment, cells were plated onto 5 mm diameter ethanol-washed coverslips and allowed to attach for the next 16 hr. A single coverslip was placed into the recording chamber (~300 μl volume) and cells were washed with isotonic external media before patch clamping.

Human promyelocytic leukemia HL-60 cells (Invitrogen, Carlsbad, CA) were cultured in suspension using 25 or 75 cm^2 flasks. The cells were maintained at 37°C in a 95% O_2/5%

CO_2 atmosphere using RPMI 1640 medium (GIBCO) supplemented with 10% Fetal Bovine Serum (FBS; Hyclone, Logan, UT, USA) and 500 μl gentamicin (10 mg/ml, GIBCO). A cell sample was dropped onto a 5 mm diameter ethanol-washed coverslip previously placed in the recording chamber. Cells were allowed to attach to the glass for 10-20 minutes before they were washed with isotonic external media and used for the experiment.

Reverse transcription polymerase chain reaction (RT-PCR) analysis of TMEM16A and ClC-3

Total RNA was isolated from HL-60 and HEK-293 cells using the Trizol reagent (Invitrogen). RNA samples were quantified using UV spectroscopy. Total RNA was treated with DNase I to remove trace amounts of genomic DNA and subsequently used in the reverse transcription reaction. The cDNA obtained was used as template for a PCR reaction carried out using the GeneAmp PCR system 9700 (*Applied Biosystems*). Primers for ClC-3 (AF172729.1) were $5'\ ^{1691}$TCGGGGCTGATTGCATTACACCT^{1713} 3′ (sense) and $5'\ ^{2198}$CACACCCGAGAACTGCCAACGATA^{2175} 3′ (antisense) and for TMEM16A (NM_018043.4) were $5'\ ^{2194}$GTTTGGCTTCGTCACCCTGTTTGT^{2217} 3′ (sense) and $5'\ ^{2603}$ACGGCGGCTCTCGGTAGTCTTTA^{2581} 3′ (antisense). Expression of the housekeeping gene transcript glyceraldehyde 3-phosphate dehydrogenase (GAPDH) was used as positive control. The predicted length for each PCR product was 508 bp for ClC3, 410 bp for TMEM16A, and 457 bp for GAPDH.

Recording solutions

External hypotonic solution contained (in mM): 139 TEACl, 0.5 $CaCl_2$, 20 HEPES; pH=7.3 with TEA-OH (292 ± 5 mOsm/kg). This hypotonic solution was used to prepare both isotonic and hypertonic solutions by adding D-mannitol. Acidic and alkaline external solutions were prepared using 20 mM MES or Bicine as pH buffers, respectively. The standard internal solution contained (in mM): 140 TEACl, 20 EGTA, 20 HEPES; pH=7.3 with TEA-OH (364 mOsm/kg). These solutions were modified by adding 20 mM MOPS or 20 mM TES instead of 20 mM HEPES to test the effects of pH buffers on channel kinetics and inactivation. Table 1 shows the composition, pH, $[Cl^-]$ and tonicity of all solutions used in this study. Tonicity values were determined using the freezing point method (VAPRO, Wescor). All chemical were purchased from Sigma-Aldrich Co., St. Louis, MO, USA.

Electrophysiological Recordings

Whole-cell currents were recorded using an Axopatch 200B amplifier and the pClamp 8 software (Molecular Devices; Sunnyvale, CA, USA). Cells were patched using glass electrodes fabricated with Corning 8161 glass (Warner Instruments, Hamdem, CT) which had a resistance of 2-4 MΩ when filled with standard internal solution. The recording chamber was grounded using an agar bridge filled with 3 M KCl. VRAC were activated by cell swelling induced after exposure to a hypotonic solution. I_{ClVol} was recorded from −80 to +120 mV in 20 mV increments using voltage clamp steps delivered every 6 s from a the holding potential of 0 mV. Currents were filtered at 2 KHz using a built-in 8 db/decade Bessel filter and then sampled at 5 KHz. Off-line analysis was done using Clampfit (Molecular Devices) as well as Origin software (OriginLab Corporation, Northampton, MA). All experiments were performed at room temperature (21-23°C).

Analysis

The absolute I_{ClVol} magnitude at the end of the voltage steps was normalized using the current magnitude measured at −80 mV, a voltage where the current-voltage relationship (I-V) was linear. Individual I-V curves were averaged and then plotted. The fraction of current decay due to H^+ or Cl^- ions is referred to as the fraction of inactivated channels (FIC) and was computed as follows:

$$FIC = \frac{I_{peak} - I_{sust}}{I_{peak}} \quad \text{Equation 1}$$

where I_{peak} and I_{sust} are current magnitudes measured at the beginning and at the end of the test pulse, respectively. FIC versus V_m curves were fit using a Boltzmann function (Equation 2)

$$FIC = FIC_{\min} + \frac{FIC_{\max} - FIC_{\min}}{1 + e^{-\frac{zF}{RT}(V_m - V_{0.5})}} \quad \text{Equation 2}$$

where FIC_{max} and FIC_{min} are the maximum and minimum FIC values, respectively, z is the apparent charge, F the Faraday constant, R the gas constant, T the temperature and $V_{0.5}$ is the V_m needed to reach $(FIC_{max}+FIC_{min})/2$. Macroscopic time constants of current decay were calculated by fitting raw current traces with a bi-exponential function:

$$I_{Cl} = Ae^{-t/\tau_1} + Be^{-t/\tau_2} + C \quad \text{Equation 3}$$

were τ_1 and τ_2 are the time constants, A, B and C are relative contributions of each component to the current decay. Current simulations were performed using the program IonChannelLab (http://www.jadesantiago.com/Electrophysiology/IonChannelLab/) developed in our laboratory.

Data are presented as mean ± SEM and n represents the number of cells tested.

Results

Volume-Regulated Chloride Currents in HEK-293 and HL-60 Cells

To characterize the effects of Cl^- and H^+ ions on the decay of whole cell chloride current (I_{ClVol}) through volume regulated anion channels (VRAC) we used HEK-293 cells (a human embryonic kidney cell line widely used for heterologous expression of ion channels) representative of non-blood cells, and HL-60 cells (a promyelocytic human leukemic cell line) as model for blood cells. In both cell types VRAC were activated by a hypotonic challenge. Fig. 1a shows I_{ClVol} from HEK-293 cells (upper panel) or HL-60 cells (lower panel) dialyzed and bathed with standard solutions containing 140 mM Cl^- and pH adjusted to 7.3. Throughout this study, we will refer to these conditions as control conditions. Raw currents recorded from the same cells under isotonic (left), hypotonic (center) and hypertonic (right) conditions are displayed. Currents were quite small under isotonic conditions (365 mosm/kg). Upon exposure to a hypotonic media (286 mosm/kg) the current increased at all membrane potentials (V_m). At negative V_m, currents from both cell types were time-independent. In contrast, at positive V_m the current rapidly decayed in HEK-293 cells but not in HL-60 cells. The I_{ClVol} decay has been referred to as inactivation and is the focus of this study. Subsequent exposure to a hypertonic media (385-392 mosm/kg) reversed the current to levels comparable to or below those observed under isotonic conditions. Current-voltage (I-V) relationships obtained under these conditions are depicted in Fig. 1b. To compare different cells, we normalized I_{ClVol} using the current magnitude obtained at -80 mV under hypotonic condition and then averaged those values. The data show that I_{ClVol} increased 2-3-fold under hypotonic condition and that this enhancement was abolished under hypertonic conditions. Furthermore, I-V curves from both

cells show the characteristic slight outward rectification previously described in other preparations [3-5,15,20,21]. In addition, the I-V curve from HEK-293 cells under hypotonic condition plateaus at positive V_m. Fig. 1c shows time courses for channel activation at +120 or -80 mV. VRAC from HEK-293 cells (upper panel) activated slower than those from HL-60 cells (lower panel). Time courses were fit with a mono-exponential function to estimate the corresponding time constant of channel activation. At +120 mV, VRAC were activated with time constants of 130 and 78 s in HEK-293 and HL-60 cells, respectively. Similar results were obtained at -80 mV (see insets).

Although the molecular identity of VRAC remains unknown several candidates have been proposed, among those TMEM16A (a Ca^{2+}-activated Cl^- channel also known as anoctacmin 1) and the ClC-3 protein [1,6-8]. Thus, we looked for the expression of both TMEM16A and ClC-3 transcripts in HEK-293 and HL-60 cells. In Fig. 2, RT-PCR experiments show that mRNA for ClC-3 is present in HEK-293 and HL-60 cells (lanes 2 and 6). Interestingly, mRNA for TMEM16A was only detected in HEK-293 cells (lane 1) as previously shown (see reference 1 for further details on characterization of TMEM16A in HEK cells). This suggests that TMEM16A is not related to VRAC in HL-60 cells.

Cl^--Dependent I_{ClVol} Decay

To understand how chloride induces I_{ClVol} decay in HEK-293 cells we carried out experiments changing the intracellular and extracellular [Cl^-]. Fig. 3a shows I_{ClVol} recordings at +120 mV obtained from four different cells dialyzed and bathed with solutions containing 25, 70, 140 or 200 mM [Cl^-]. A larger I_{ClVol} decay was observed when the [Cl^-] was higher. As the [Cl^-] increased the I-V curves became less linear (Fig. 3b) and the fraction of inactivated channels (FIC) increased at positive V_m (Fig. 3c). In consequence, at +120 mV the FIC value was 0.48 ±0.05 with 200 mM Cl^- but decreased to 0.08±0.02 when [Cl^-] was reduced to 25 mM. Next, we determined the relative contribution of internal and external Cl^- to I_{ClVol} decay by separately changing the [Cl^-] while keeping the pH= 7.3 on both sides of the membrane. When $[Cl^-]_i$ was decreased from 140 mM to 70 and then to 25 mM in separate cells (Fig. 3d), the FIC at +120 mV decreased in a similar manner from 0.57±0.04 to 0.33±0.04 to 0.11±0.03, respectively. This result resembled that obtained when [Cl^-] was decreased in a symmetric fashion (Fig. 3c). In contrast, reducing $[Cl^-]_e$ from 140 to 25 mM slightly increased FIC at potentials between +40 to +60 mV but not between +80 to +120 mV (Fig. 3e). The FIC data were analyzed using a Boltzmann equation (Equation 2). Data shown in Fig. 3c were fit using an apparent gating charge z=1.4 and a $V_{0.5}$=97 mV (continuous lines), where $V_{0.5}$ is the voltage needed to reach half FIC. Similarly, data show in Fig. 3d were fit with z=1.4 and $V_{0.5}$ value that ranged between 80 to 100 mV (continuous lines).

H^+-Dependent I_{ClVol} Decay

Previous work on cultured cells reported that external H^+ modulates I_{ClVol} decay [23,26]. To further understand the modulatory effect of H^+ ions, we assayed the effect of H^+ on I_{ClVol} decay by varying the external pH between 5.5 and 9. Fig. 4a shows raw I_{ClVol} traces recorded at +120 mV from a HEK-293 cell dialyzed with the standard internal solution containing 140 mM Cl^- and bathed in a hypotonic solution containing 140 mM Cl^- whose pH was adjusted to 7.3 or 5.5. In this experiment FIC increased from 0.57 to 0.84 but on average the FIC increased from 0.33±0.05 when pH_e was 7.3 (n=58) to 0.60±0.05 when pH_e was 5.5 (n=13). In addition, I_{ClVol} decayed faster in cells bathed in an acidic media. Fitting I_{ClVol} with a double exponential function (equation 3) gave fast and slow time constants whose values were 134±44 and 2197 ±457 ms at pH= 7.3, while at pH= 5.5 these values became 104±31 and 534±55 ms. Fig. 4b depicts FIC as a function of V_m at pH 5.5, 7.3 and 9. Therefore, FIC increased as the V_m became positive and as the pH_e became acidic. At pH_e 9.0, the inactivation was nearly abolished. The

V_m-dependent effects of H^+ on I_{ClVol} decay were fit with equation 2 (continuous lines in Fig. 4b) using z=1.25 and $V_{0.5}$= 78 or 65 mV for pH=7.3 or 5.5 and 9.0.

It is known that HEPES buffer but not TES, inhibits the outwardly rectifying anion channel [10]. Since the pH of our experimental solutions was buffered with HEPES, we tested whether the I_{ClVol} decay could be related to channel block by HEPES. To this end we prepared internal and external solutions (isotonic, hypotonic and hypertonic) containing 140 mM Cl^- and pH buffered to 7.3 with either 20 mM HEPES, 20 mM MOPS or 20 mM TES (solutions A_i, A_{e1}, A_{e2}, A_{e3}, B_i, B_{e1}, B_{e2}, B_{e3}, C_i, C_{e1}, C_{e2} and C_{e3}; see Table 1). I_{ClVol} was recorded at +120 mV from HEK-293 cells consecutively bathed in isotonic, hypotonic and hypertonic solutions. FIC values determined as described above were 0.55±0.05, 0.53±0.04 and 0.52±0.06 with HEPES (n=6), MOPS (n=7) and TES (n=7), respectively. The corresponding fast/slow time constants of inactivation were 315±70/1571±225, 225±66/1329±139 and 126±18/1510±179 ms. Thus, I_{ClVol} decay in HEK cells was not affected by the pH buffer used.

In other Cl^- channels, such as ClC-type channels the H^+ effect on gating is influenced by the $[Cl^-]$ [17]. To determine whether or not the H^+ effects on I_{ClVol} decay were also dependent on $[Cl^-]$, the cells were dialyzed and bathed in solutions containing only 25 mM Cl^-. This condition blunts the Cl^--dependent inactivation (Fig. 3c) and should unmask the H^+-dependent inactivation. Fig. 4c shows raw I_{ClVol} obtained at +120 mV from a cell bathed in a solution containing 25 mM $[Cl^-]$ with pH 7.3 that was changed to a solution with pH 5.5. I_{ClVol} showed little decay at pH_e= 7.3, however, a larger decay was apparent at pH_e= 5.5. The results are summarized in Fig. 4d, where FIC values obtained at pH_e= 5.5, 7.3 and 9.0 are plotted as a function of V_m. The maximum FIC value at pH_e 5.5 was 0.36 while no difference was observed when pH_e was 7.3 or 9.0. From fitting the data with equation 2, a z value of 0.95 was estimated. Therefore in HEK-293 cells increasing the $[H^+]_e$ under low $[Cl^-]$ enhances VRAC inactivation. Since in HL-60 cells I_{ClVol} did not decay with 140 mM Cl^- (Fig. 1a) we used this condition to further analyze the effects of external H^+ on I_{ClVol} decay. Fig. 5a shows raw current traces recorded at +120 mV from HL-60 cells exposed to pH 7.3 and then pH 5.5 (left) or 7.3 and then 9.0 (right). Low pH_e induced slight inactivation while pH 9.0 did not. Fig. 5b summarizes our findings. Fitting the data with equation 2 we estimated an apparent gating charge of z=1.1 and a maximum FIC value of 0.37. Comparatively, pH_e 5.5 induced less inactivation in HL-60 cells than in HEK-293 cells.

Effect of external Cl^- ions on I_{ClVol} at pH_e 9.0

Alkaline pH_e nearly abolished I_{ClVol} inactivation in HEK-293 cells even when the $[Cl^-]$ on both sides of the membrane was 140 mM (Fig. 4b). Thus, we re-examined the role of external Cl^- ions on inactivation under alkaline conditions to minimize the contribution of the pH_e. Fig. 6a shows raw I_{ClVol} recorded from the same cell exposed to a hypotonic solution containing initially 140 mM Cl^- on both sides of the membrane and pH= 7.3. Under this condition, I_{ClVol} decayed approximately 45%. When the pH_e was increased to 9.0, there was a reduction on current decay. Additionally, I_{ClVol} decayed even less when the $[Cl^-]_e$ was reduced from 140 to 25 while keeping the pH_e at 9.0. Fig. 6b shows FIC vs V_m curves that summarize the effects of simultaneously increasing pH_e and decreasing $[Cl^-]_e$ on inactivation. Increasing pH_e from 7.3 to 9.0 decreased FIC at all V_m. Decreasing $[Cl^-]_e$ from 140 to 25 further decreased FIC at positive V_m. Continuous lines are fits with equation 2 using z=2.53 and $V_{0.5}$ values between 77 and 86 mV. Maximum FIC obtained from the fit were 0.62, 0.45 and 0.28 when pH_e/$[Cl^-]_e$ were 7.3/140, 9.0/140 and 9.0/25, respectively.

Kinetic Model

The data shown in Fig. 3 suggest that intracellular Cl^- ions interact with the channel to facilitate V_m-dependent inactivation. In addition, Fig. 4 and 5 show that H^+ have effects on I_{ClVol} decay

too and those effects are concentration- and V_m-dependent, just as the effects of $[Cl^-]_i$. The fact that the H^+ effects were largely diminished by lowering $[Cl^-]$ (Fig. 4c,d) suggests that both effects are coupled. Based in these observations we tried to represent the effects of internal Cl^- and external H^+ on I_{ClVol} decay (Fig. 7) using a kinetic model. This model assumed the existence of external and internal binding sites (upper left corner, dash circles) for the H^+ (*red circle*) and Cl^- (*blue circle*) ions. The interactions between the protein and the ions are described by the equilibrium constants K_H and K_{Cl}, respectively. Since our data show that an increase in $[H^+]_e$ and $[Cl^-]_i$ produce enhancement as well as acceleration of I_{ClVol} decay, our model assumes that binding of H^+ and Cl^- ions (Fig. 7, outer layer) to the channel facilitate I_{ClVol} decay. If the ion binding sites are located within the electrical field, then negative V_m would increase occupancy of the sites by attracting H^+ and pushing Cl^- into the pore whereas positive V_m would reduce occupancy by repelling H^+ and keeping Cl^- in the citosol. Thus, a negative electric field would induce a large FIC and a positive electric field would induce a small FIC, however, the opposite was observed in our experiments. For that reason, we propose that both binding sites are outside the electrical field, therefore K_{Cl} and K_H can be V_m-independent. The idea of V_m-independent external binding sites has already been postulated by Nilius and co-workers based on their own experimental observations [16,26]. Our data show that FIC was V_m-dependent, thus we introduced the voltage dependence of inactivation in the model by including two V_m-dependent rate constants: α_v and β_v These rate constants are associated with transitions that connect two unknown conformational states shown in the outer and central layers of the model (Fig. 7). Thus, in the model we assume that the role of chlorination and protonation is to induce a conformational change from where an additional V_m-dependent rearrangement leads the channel to states prompt to inactivate (central layer). Previously, it was proposed that occupancy of a site within the VRAC pore might prevent channel closing [26]. To incorporate this idea in our model, we represented a fully inactivated channel as an empty, collapsed pore with one H^+ and one Cl^- bound (third layer). The parameter values that describe the transitions between states (listed in Table 2) were estimated by trial and error and finally adjusted during the simulation procedure. Simulations of whole cell currents using our model are displayed in Fig. 8. The model qualitatively reproduced: I_{ClVol} time course at different V_m (Fig. 8a), FIC vs V_m at different $[Cl^-]_i$ (Fig. 8b), the FIC vs V_m at various pH_e with $[Cl^-]_i$ = 140 mM (Fig. 8c) and FIC vs V_m at various pH_e with $[Cl^-]_i$ = 25 mM (Fig. 8d). Data show in Fig. 8b, 8c and 8d were fit with equation 2. The resulting z and $V_{0.5}$ values are compared in Table 3 with those obtained from fitting our experimental data collected under diverse ionic conditions.

Discussion

VRAC channels have been functionally identified in all mammalian cells. A prominent property is their lack of or little voltage-dependence, as well as I-V relationships that display slight outward rectification in some cell types [15,18]. At depolarized voltages VRAC currents show a time-dependent decay in non-blood cells which has been associated with an "inactivation" process [18]. Unlike the classical inactivation of voltage-gated Na^+ or K^+ channels, inactivation in VRAC may be triggered initially by ions and subsequently by voltage. In this work, we have explored the role of H^+ and Cl^- ions as causal agents for voltage-dependent inactivation in VRAC.

Our findings extend previous observations in BC_3H1 myoblasts which showed that low pH_e accelerates VRAC inactivation with only a marginal effect on current amplitude [26]. Later it was demonstrated that in CEPAE cells the unitary current amplitude is increased by low pH_e which could account for the increase in whole-cell current but could not explain the increase on the rate of inactivation [19]. Our results are in agreement with the observation that an increased external $[H^+]$ accelerates current decay and produces a slight increase in current amplitude. In addition, we show here that an acidic pH_e is able to increase the fraction of

inactivated channels when symmetrical [Cl^-] is high. However, our data also show that decreasing the $[Cl^-]_i$ drastically diminishes inactivation regardless of the $[Cl^-]_e$, thus suggesting that internal Cl^- ions have a dominant role in VRAC inactivation.

It is interesting to note that VRAC from HEK-293 cells are functionally different from VRAC native to HL-60 cells. VRAC from HL-60 cells as well as those from human neutrophils and T lymphocytes display little current decay [12,20,25]. In agreement with these reports we observed very little decay in HL-60 cells even when the pH_e was decreased to 5.5 (intracellular Cl^- was 140 mM). Moreover, the degree of I_{ClVol} decay was similar to that observed in HEK-293 cells recorded in symmetrical 25 mM Cl^-. Thus, it seems as if VRAC from HL-60 cells lack inactivation due to intracellular Cl^-. This observation and the fact that the single channel conductance of VRAC from blood cells is smaller than that of other mammalian cells [15] might indicate that these two channels are encoded by different, yet unknown,molecular entities. Since our results indicate that HEK-293 and HL-60 cells express the ClC-3 mRNA and that ablation of ClC-3 did not eliminated the hypotonicity activated Cl^- currents [2,24], then it is quite likely that the ClC-3 protein is not VRAC. On the other hand, it has been recently suggested that TMEM16A, a Ca^{2+}-activated Cl^- channel, could be a crucial component of VRAC in epithelial cells [1]. Interestingly, we detected mRNA for TMEM16A in HEK-293 (see reference 1 for further details) but not in HL-60 cells. Although, this implies that TMEM16A is not part of VRAC in HL-60 cells, our evidence is not sufficient to conclude that TMEM16A cannot work as a VRAC in other cells including HEK-293 cells. Therefore, different gene(s) could be responsible for VRAC channels in HL-60 or other blood cells.

The H^+ and Cl^- effects on VRAC inactivation are reminiscent of the effects these ions have on ClC chloride channels. It has been proposed that ClC channels gain voltage sensitivity via interaction with H^+ ions and such interaction can be modulated by Cl^- ions [13,17]. Thus, to explain inactivation we propose that VRAC have binding sites for both H^+ and Cl^- ions. Since our data suggest that the H^+ and Cl^- effects are coupled we assumed that both ions are needed to trigger the inactivation process. Previous observations showing that high $[Cl^-]_e$ or highly permeable anions prevented inactivation [26] suggested that pore occupancy also plays a role. To explain VRAC inactivation we incorporated these ideas into a kinetic model. In our model a full open conformation is reached when binding sites for H^+ and Cl^- are occupied (Fig. 7, lower right corner of outer layer). From this conformation, channels can reach the inactivated state through a V_m-dependent conformational change controlled by voltage-dependent rate constants α_v and β_v. Inactivation would be enhanced when the external H^+ and internal Cl^- binding sites are occupied and the pore is empty. This hypothesis was tested by simulating pore occupancy with the help of our model. Supplemental Fig. 9 shows that the pore remains open when one permeant anion is bound to a site located at an electrical distance of 0.2 from the outside. However, when the pore is empty inactivation would occur due to a collapse of the pore. For example, assuming that $[Cl^-]_e=[Cl^-]_i$= 140 mM we calculated P_u (probability that the pore is unpopulated) values of 0.02 and 0.48 at -100 and +100 mV, respectively. These numbers are compatible with our experimental observations (compare data in Fig. 3 and 4 with Fig. 8). Hence our model predicts that lowering $[Cl^-]_e$ from 140 to 20 mM will slightly enhance inactivation at positive V_m (Supplemental Fig. 9a) and helps explain the V_m and external Cl^- dependence of inactivation (Supplemental Fig. 9b). Although limited, our model is the first to reproduce both the time course of I_{ClVol} as well as the H^+ and Cl^- effects on inactivation.

In summary, we show that the decay of I_{ClVol} in non-blood cells depends on the interaction of intracellular Cl^- and external H^+ ions as well as the pore occupancy. The ions interact with the channel outside the electrical field to induce a conformational change that prompts the channels to inactive in a V_m-dependent manner. This ion- dependent inactivation might be relevant for VRAC function since the H^+ and Cl^- effects occurred within a physiological range of concentrations.

Supplementary Material

Refer to Web version on PubMed Central for supplementary material.

Acknowledgments

This work was supported by grants 79897, 59889 and 45895 (Consejo Nacional de Ciencia y Tecnologia, Mexico) and PO1-HL18208 (National Institutes of Health, USA). TRS and JADSC received a scholarship from Consejo Nacional de Ciencia y Tecnologia, Mexico.

References

1. Almac J, Tian Y, Aldehni F, et al. TMEM16 proteins produce volume-regulated chloride currents that are reduced in mice lacking TMEM16A. J Biol Chem 2009;284:28571–28578. [PubMed: 19654323]
2. Arreola J, Begenisich T, Nehrke K, et al. Secretion and cell volume regulation by salivary acinar cells from mice lacking expression of the Clcn3 Cl- channel gene. J Physiol 2002;545:207–216. [PubMed: 12433961]
3. Arreola J, Hallows KR, Knauf PA. Volume-activated chloride channels in HL-60 cells: potent inhibition by an oxonol dye. Am J Physiol 1995;269:C1063–C1072. [PubMed: 7485447]
4. Arreola J, Melvin JE, Begenisich T. Volume-activated chloride channels in rat parotid acinar cells. J Physiol 1995;484:677–687. [PubMed: 7623284]
5. Arreola J, Park K, Melvin JE, et al. Three distinct chloride channels control anion movements in rat parotid acinar cells. J Physiol 1996;490:351–362. [PubMed: 8821134]
6. Coca-Prados M, Sánchez-Torres J, Peterson-Yantorno K, et al. Association of ClC-3 channel with Cl^- transport by human nonpigmented ciliary epithelial cells. J Membr Biol 1996;150:197–208. [PubMed: 8661780]
7. Duan D, Winter C, Cowley S, et al. Molecular identification of a volume-regulated chloride channel. Nature 1997;390:417–421. [PubMed: 9389484]
8. Duan D, Zhong J, Hermoso M, et al. Functional inhibition of native volume-sensitive outwardly rectifying anion channels in muscle cells and Xenopus oocytes by anti-ClC-3 antibody. J Physiol 2001;531:437–444. [PubMed: 11230516]
9. Furst J, Gschwentner M, Ritter M, et al. Molecular and functional aspects of anionic channels activated during regulatory volume decrease in mammalian cells. Pflugers Arch 2002;444:1–25. [PubMed: 11976912]
10. Hanrahan JW, Tabcharini JA. Inhibition of an outwardly rectifying anion channel by HEPES and related buffers. J Memb Biol 1990;116:65–77.
11. Hille, B. Ion Channels of Excitable Membranes. Sinauer Associates, Inc.; USA: 2001.
12. Lewis RS, Ross PE, Cahalan MD. Chloride channels activated by osmotic stress in T lymphocytes. J Gen Physiol 1993;101:801–26. [PubMed: 7687269]
13. Meyer K, Korbmacher C. Cell swelling activates ATP-dependent voltage-gated chloride channels in M-1 mouse cortical collecting duct cells. J Gen Physiol 1996;108:177–193. [PubMed: 8882862]
14. Miller C. ClC chloride channels viewed through a transporter lens. Nature 2006;440:484–489. [PubMed: 16554809]
15. Nilius B, Eggermont J, Voets T, et al. Properties of volume-regulated anion channels in mammalian cells. Prog Biophys Mol Biol 1997;68:69–119. [PubMed: 9481145]
16. Nilius B, Prenen J, Droogmans G. Modulation of volume-regulated anion channels by extra- and intracellular pH. Pflugers Arch 1998;436:742–748. [PubMed: 9716708]
17. Niemeyer MI, Cid LP, Yusef YR, et al. Voltage-dependent and -independent titration of specific residues accounts for complex gating of a ClC chloride channel by extracellular protons. J Physiol 2009;587:1387–1400. [PubMed: 19153159]
18. Okada Y. Cell volume-sensitive chloride channels: phenotypic properties and molecular identity. Contrib Nephrol 2006;152:9–24. [PubMed: 17065805]
19. Okada Y, Sato K, Numata T. Pathophysiology and puzzles of the volume-sensitive outwardly rectifying anion channel. J Physiol 2009;587:2141–2149. [PubMed: 19171657]

20. Perez-Cornejo P, Arreola J, Law FY, et al. Volume-sensitive chloride channels do not mediate activation-induced chloride efflux in human neutrophils. J Immunol 2004;172:6988–6993. [PubMed: 15153519]

21. Poletto Chaves LA, Varanda WA. Volume-activated chloride channels in mice Leydig cells. Pflugers Arch 2008;457:493–504. [PubMed: 18574591]

22. Rossow CF, Duan D, Hatton WJ, et al. Functional role of amino terminus in ClC-3 chloride channel regulation by phosphorylation and cell volume. Acta Physiol (Oxf) 2006;187:5–19. [PubMed: 16734738]

23. Sabirov RZ, Prenen J, Droogmans G, et al. Extra- and Intracellular Proton-Binding Sites of Volume-Regulated Anion Channels. J Memb Biol 2000;177:13–22.

24. Stobrawa SM, Breiderhoff T, Takamori S, et al. Disruption of ClC-3, a chloride channel expressed on synaptic vesicles, leads to a loss of the hippocampus. Neuron 2001;29:185–196. [PubMed: 11182090]

25. Stoddard JS, Steinbach JH, Simchowitz L. Whole cell Cl- currents in human neutrophils induced by cell swelling. Am J Physiol 1993;265:C156–C165. [PubMed: 8338124]

26. Voets T, Droogmans G, Nilius B. Modulation of Voltage-dependent Properties of a Swelling-activated Cl Current. J Gen Physiol 1997;110:313–325. [PubMed: 9276756]

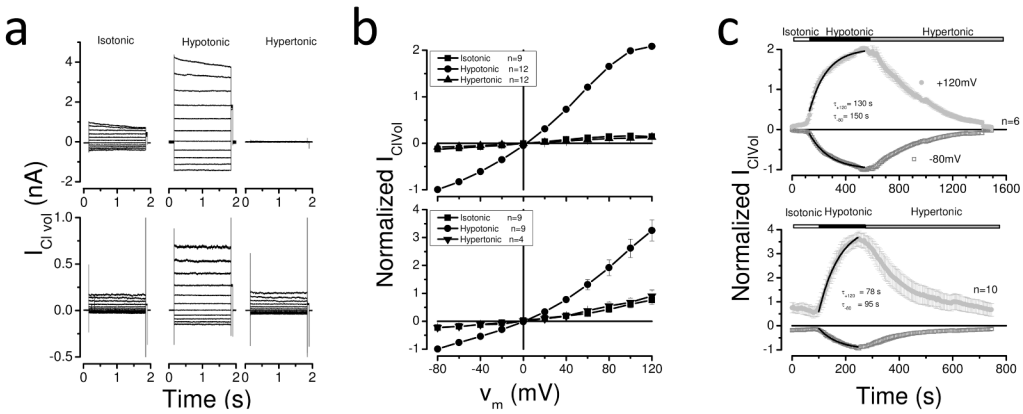

Fig. 1. Activation of volume-regulated chloride channels in HEK-293 and HL-60 cells by a hypotonic solution

a Raw traces obtained from individual HEK-293 (upper raw) and HL-60 (lower raw) cells sequentially exposed to isotonic (left), hypotonic (middle) and hypertonic (right) media. Voltage steps between -80 and +120 mV in 20 mV increments delivered from a holding voltage of 0 mV were used to elicit currents. **b** I-V relationships from HEK-293 (upper) or HL-60 (lower) cells under isotonic (*black boxes*), hypotonic (*black circles*) and hypertonic (*black triangles*) conditions. **c** Time course of I_{ClVol} activation in HEK-293 cells (upper; n=6) or HL-60 (lower, n=10) cells at +120 or -80 mV. The sequential order of perifused solutions is indicated by upper bars. Continuous black lines on top of symbols are mono-exponential fits used to estimate activation time constants (inserted). In b and c, I_{ClVol} amplitude was normalized using the current measured at -80 mV under hypotonic conditions. Experimental conditions included $[Cl^-]_i = [Cl^-]_e$ =140 mM and $pH_i = pH_e = 7.3$ (solutions A_i, A_{e1}, A_{e2} and A_{e3}).

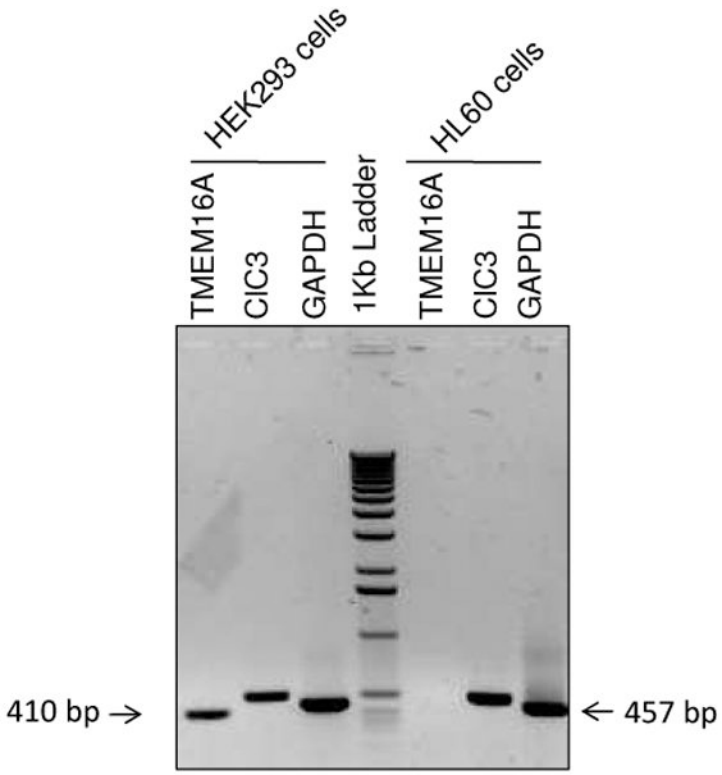

Fig. 2. RT-PCR analysis of TMEM16A (NM_018043.4) and ClC-3 (AF172729.1) transcripts in HEK-293 (lanes 1-3) and in HL-60 (lanes 5-7) cells

Lanes 1 and 5: TMEM16A. Lanes 2 and 6: ClC-3. Lane 3 and 7: GAPDH, positive control. Lane 4: 1Kb DNA ladder. The expected length of the PCR products was 410 bp for TMEM16A, 508 bp for ClC3 and 457 bp for GAPDH. Experiments were carried out by triplicate.

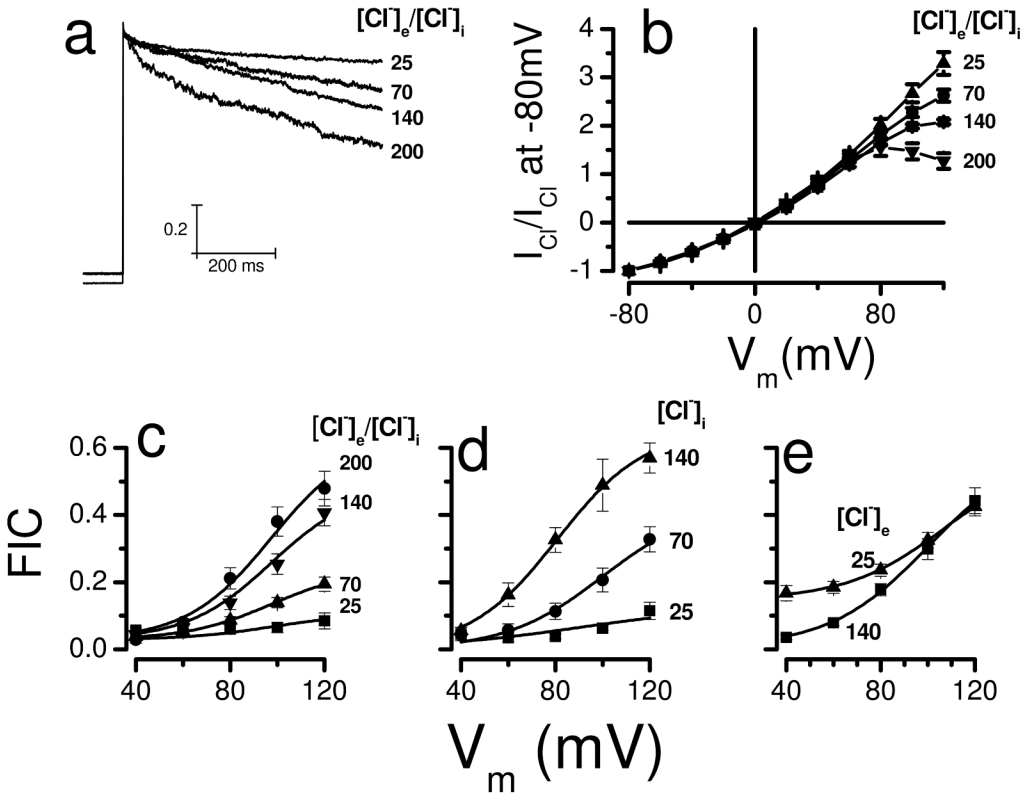

Fig. 3. Effect of $[Cl^-]$ on $I_{Cl,Vol}$ decay in HEK-293 cells

a Normalized I_{ClVol} recorded at +120 mV from 4 different cells bathed and dialyzed with solutions containing 25, 70, 140 and 200 mM Cl^-. Hypotonic solutions used to activate I_{ClVol} were prepared by removing D-mannitol from the corresponding isotonic solutions. **b** Normalized I-V relationships at the indicated [Cl]. I_{ClVol} magnitudes were measured at the end of each voltage step and normalized to the I_{ClVol} magnitude measured at -80 mV. **c** FIC vs V_m curves as a function of $[Cl^-]_i = [Cl^-]_e = 200$ (*black circles*, n=6), 140 (*down triangles*, n=12), 70 (*up triangles*, n=10) and 25 mM (*black boxes*, n=4). Solutions used in panels a, b and c were A_i, A_{e1}, A_{e2}, A_{e3}, F_i, F_{e1}, F_{e2}, F_{e3}, G_i, G_{e1}, G_{e2}, G_{e3}, H_i, H_{e1}, H_{e2} and H_{e3}. **d** FIC vs V_m curves as a function of $[Cl^-]_i$ (140mM, *up triangles*, n=15; 70 mM, *black circles*, n=9, or 25 mM, *black boxes*, n=6) when $[Cl^-]_e$ was 140 mM. Continuous lines are fits with equation 2. Solutions used: A_i, A_{e1},Ji and K_i. **e** Curves of FIC vs V_m at $[Cl^-]_e$ of 140 (*black boxes*, n=12) or 25 mM (*up triangles*, n=9). In all cases $[Cl^-]_i$ was 140 mM while $pH_i = pH_e = 7.3$ (solutions A_i, A_{e1} and I_{e2}).

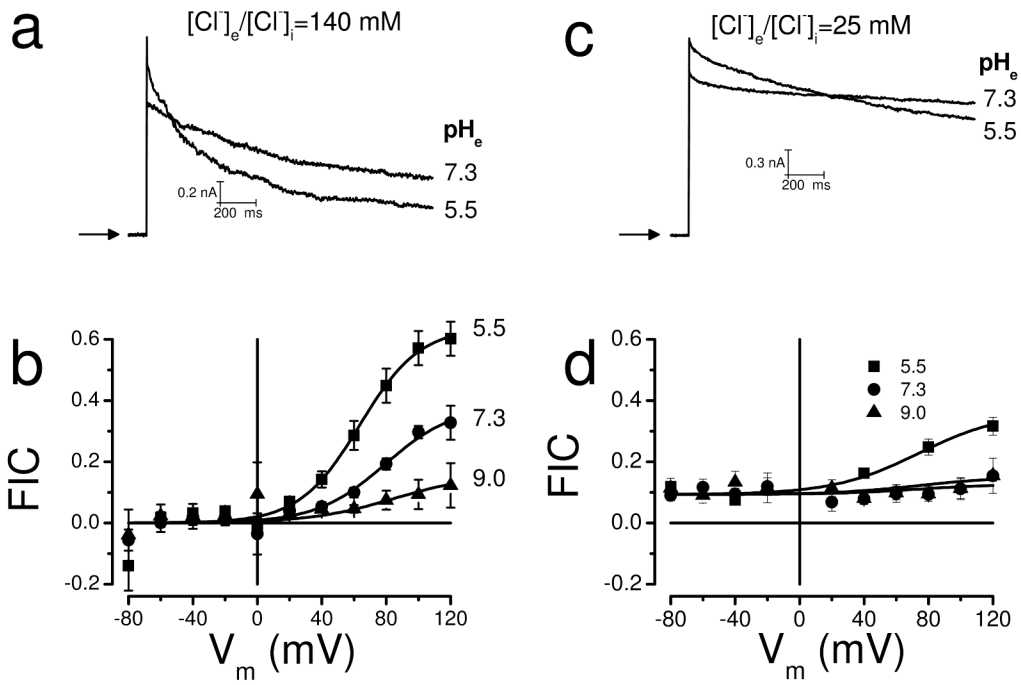

Fig. 4. pH_e effects on $I_{Cl,Vol}$ decay in HEK-293 cells show $[Cl^-]$-dependence

a Raw I_{ClVol} traces recorded at +120 mV from the same cell dialyzed and bathed in solutions containing 140 mM Cl^- whose pH_e was adjusted to 7.3 or to 5.5 (solutions A_i,A_{e1},D_{e1}). pH_i was 7.3. **b** Curves of FIC vs V_m as a function of pH_e (5.5, n=13; 7.3, n=23 and 9.0, n=10). Continuous lines are fits with equation 2. Solutions used: A_i, A_{e1}, D_{e1}, E_{e1}. **c** Raw I_{ClVol} traces recorded at +120 mV from the same cell bathed and dialyzed with solutions containing 25 mM Cl^- whose pH_e was adjusted to 7.3 or to 5.5 (solutions G_i, G_{e1} and G_{e4}). **d** FIC vs V_m curves as a function of pH_e of 5.5 (*black boxes*, n=14), 7.3 (*black circles*, n=21) and 9.0 (*black triangles*, n=7). Solutions used: G_i, G_{e1}, G_{e4} and G_{e5}.

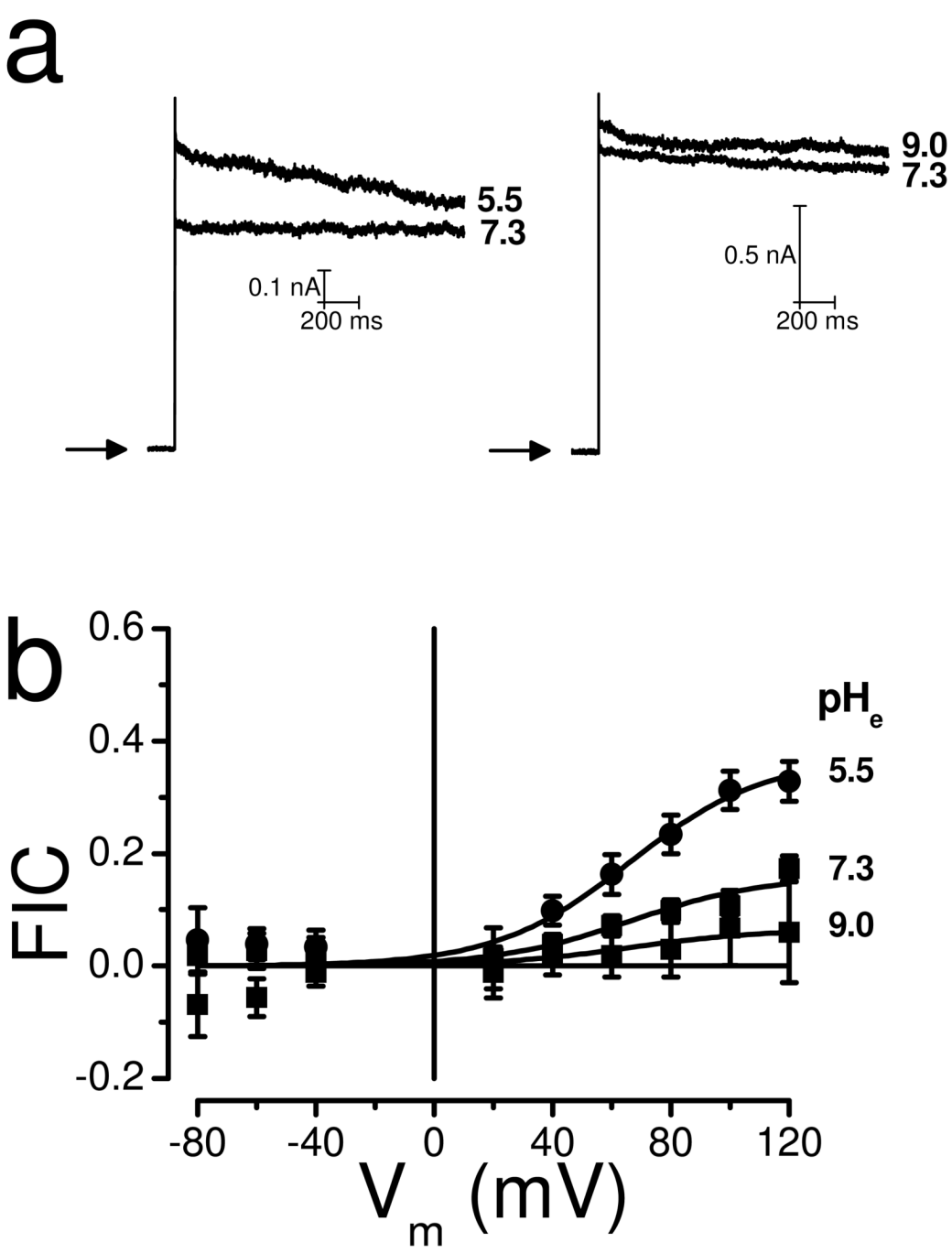

Fig. 5. Effect of pH_e on I_{ClVol} from HL-60 cells

a Raw I_{ClVol} traces obtained at +120 mV from two different cells sequentially bathed with solutions whose pH were 7.3 and 5.5 (left) or 7.3 and 9.0 (right). **b** Curves of FIC vs V_m at the indicated pH_e. In all cases $[Cl^-]_i = [Cl^-]_e = 140$ mM and $pH_i = 7.3$ (solutions A_i, A_{e1}, D_{e1} and E_{e1}). The total number of experiments was 9, 20 and 8 for solutions with pH_e 5.5, 7.3 and 9.0, respectively. Continuous lines are fits with equation 2

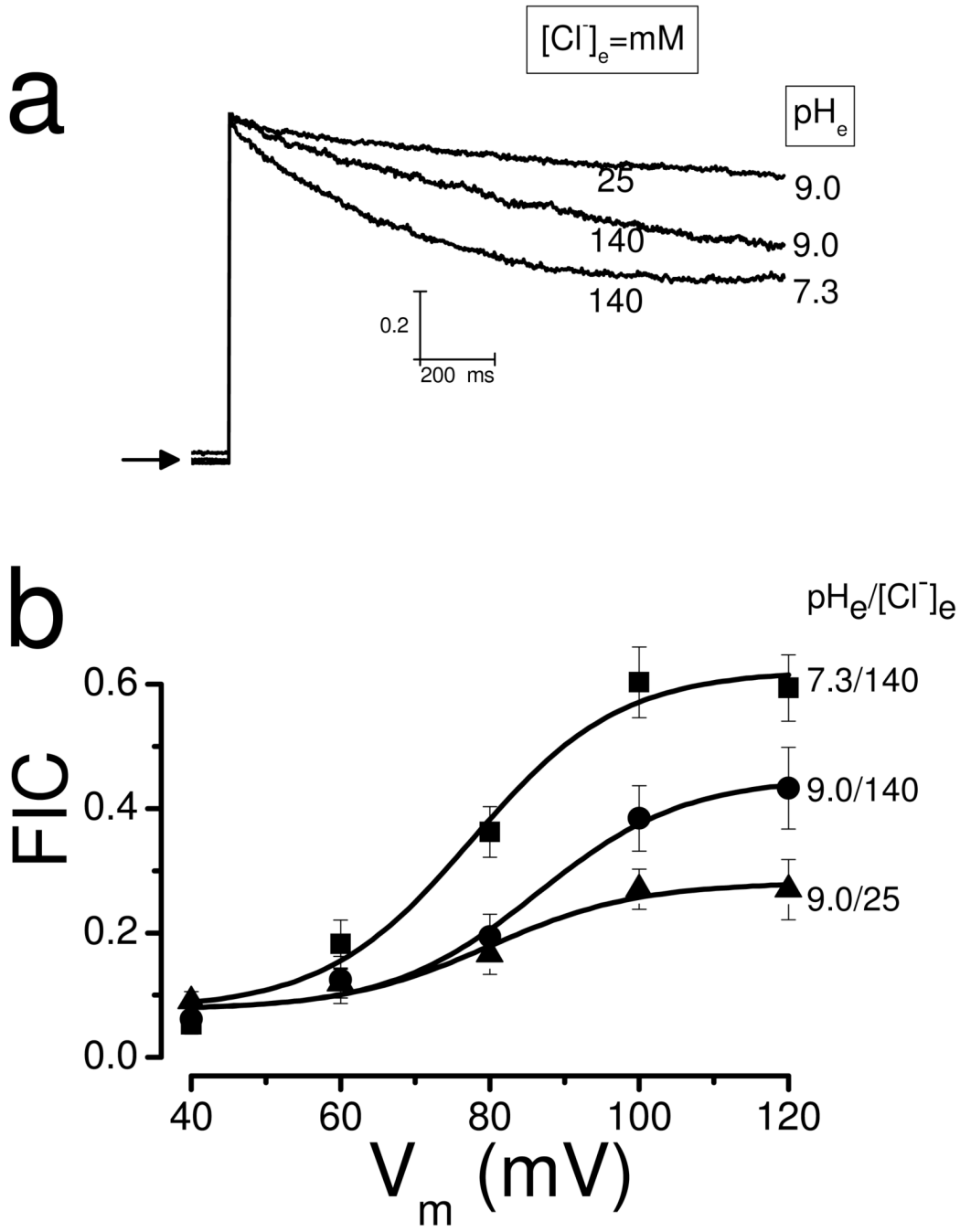

Fig. 6. Effect of low $[Cl^-]_e$ on I_{ClVol} decay in HEK-293 cells bathed in alkaline media

a Raw I_{ClVol} traces recorded at + 120 mV from the same cell exposed to hypotonic solutions containing 140 mM Cl^- and pH = 7.3, 140 mM Cl^- and pH = 9.0 and 25 mM Cl^- and pH = 9.0. **b** Curves of FIC vs V_m as a function of $pH_e/[Cl^-]_e$ = 7.3/140mM (*black circle*), 9.0/140 mM (*black boxes*) and 9.0/25 (*black triangles*) are shown (solutions A_i, A_{e1}, E_{e1} and I_{e3}). In all experiments $[Cl^-]_i$ = 140 mM, pH_i = 7.3 and n=11

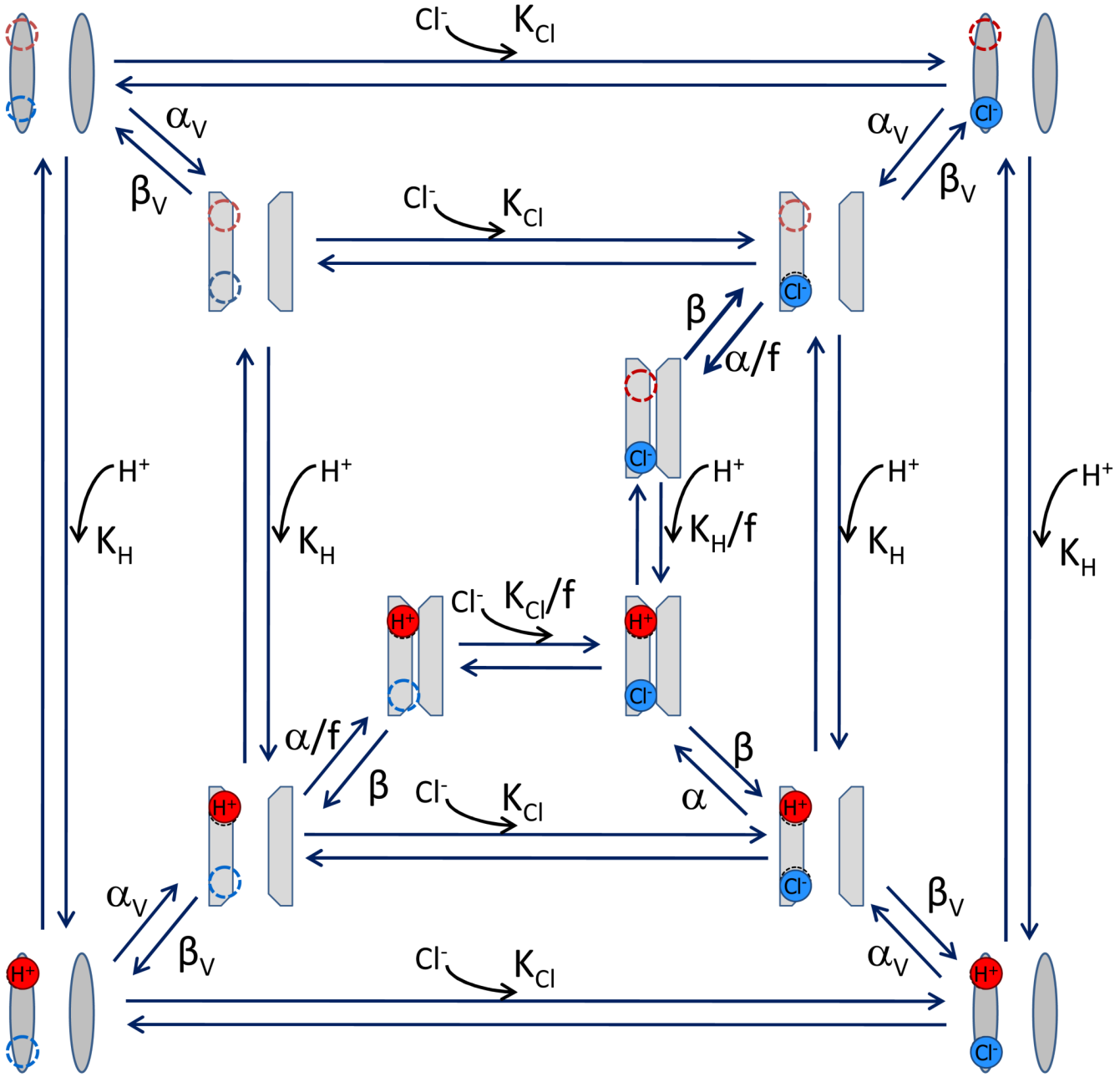

Fig. 7. A kinetic model to describe VRAC inactivation

This model is based on the dependence of FIC with the $[H^+]_e$ and $[Cl^-]_i$. Dash circles are external and internal binding sites for H^+ *(red circle)* and Cl^- (*blue circle*), respectively. An open channel conformation can be reached when both binding sites are occupied (lower right corner of outer layer) but if this is followed by a V_m-dependent conformational change characterized by rate constants α_v and β_v then the channel inactivates. Inactivation states (inner most layer) are represented by a collapsed pore with either one or both binding sites occupied. Here, K_H and K_{Cl} are the equilibrium constant for binding of H^+ and Cl^-, respectively. f is a scale factor

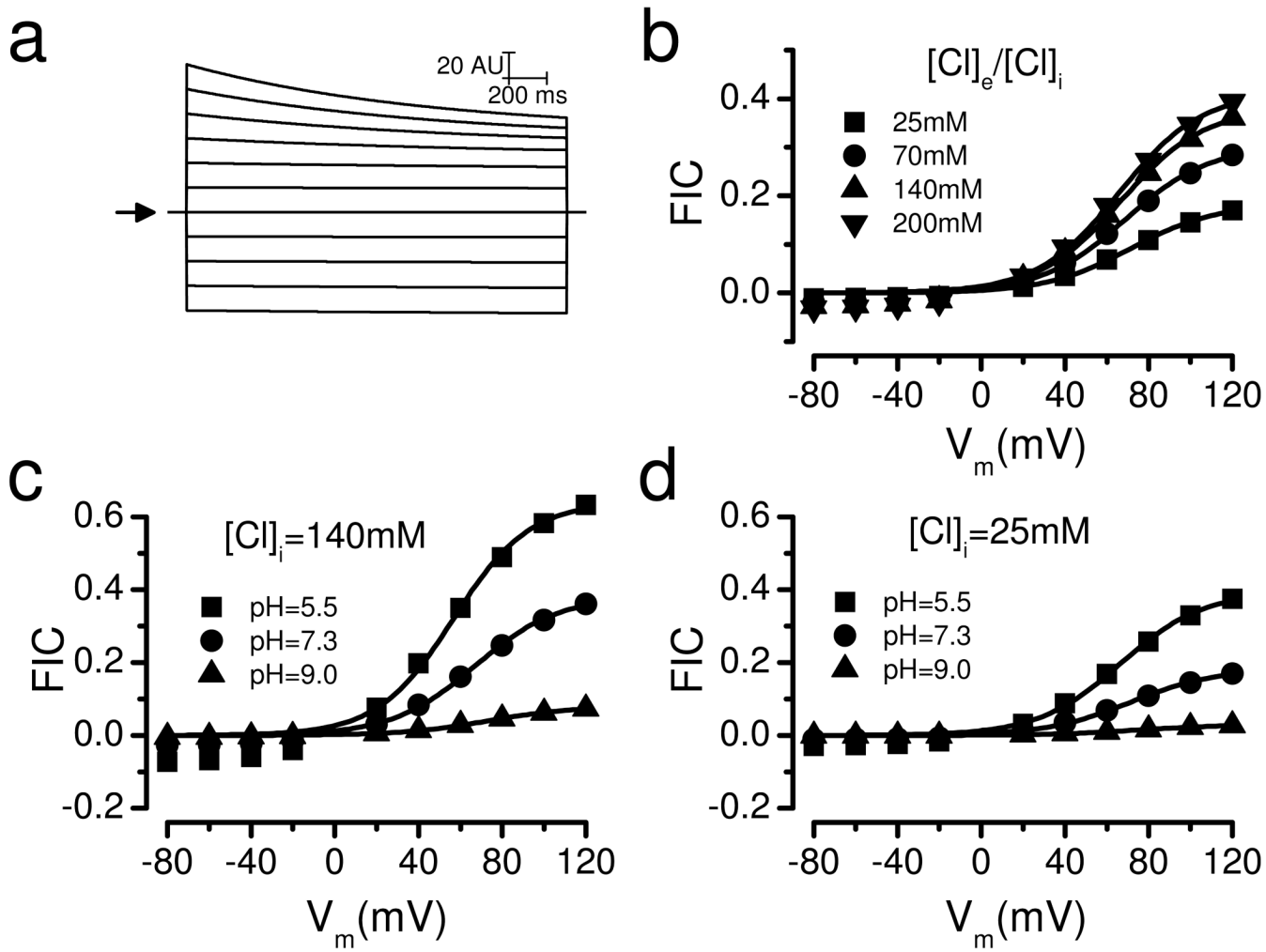

Fig. 8. Simulation of I_{ClVol} time course and ion-dependence of I_{ClVol} decay

a Time course of I_{ClVol} between -80 and +120 mV was simulated using the model shown in Fig. 7 and the rate constants listed in Table 2. **b** FIC vs V_m curves as a function of $[Cl^-]_i$ (25, 70, 140 and 200mM) were also simulated. Continuous lines are fits with equation 2 using z=1.43. **c** and **d**: Simulations of FIC vs V_m as a function of pH_e (5.5, 7.3, and 9.0) and $[Cl^-]_i$ (140 mM, c or 25 mM, d). Continuous lines are fits with equation 2 using z=1.53 and 1.44 for 140 and 25 mM $[Cl^-]_i$, respectively

Table 1

Composition, pH and osmolarities of internal and external solutions

Internal solutions are labeled with subscript i. External solutions are labeled with subscript e1, e2 and e3 that stand for hypotonic, isotonic and hypertonic bathing solutions, respectively.

Solution	Composition (mM)					pH	Osmolality (mOsm/Kg)
	TEACl	EGTA	$CaCl_2 \cdot 2H_2O$	D- Mannitol	Buffer (20 mM)		
A_i	140	20	0.0	0.0	HEPES	7.3	355.0 ± 5.0
A_{e1}	139	0.0	0.5	0.0	HEPES	7.3	292± 5.0
A_{e2}	139	0.0	0.5	90	HEPES	7.3	375± 5.0
A_{e3}	139	0.0	0.5	110	HEPES	7.3	393± 5.0
B_i	140	20	0.0	0.0	MOPS	7.3	353
B_{e1}	139	0.0	0.5	0.0	MOPS	7.3	287
B_{e2}	139	0.0	0.5	90	MOPS	7.3	387
B_{e3}	139	0.0	0.5	110	MOPS	7.3	401
C_i	140	20	0.0	0.0	TES	7.3	361
C_{e1}	139	0.0	0.5	0.0	TES	7.3	286
C_{e2}	139	0.0	0.5	90	TES	7.3	377
C_{e3}	139	0.0	0.5	110	TES	7.3	406
D_i	140	20	0.0	0.0	MES	5.5	355
D_{e1}	139	0.0	0.5	0.0	MES	5.5	283
D_{e2}	139	0.0	0.5	90	MES	5.5	370
D_{e3}	139	0.0	0.5	110	MES	5.5	390
E_i	140	20	0.0	0.0	BICINE	9.0	355
E_{e1}	139	0.0	0.5	0.0	BICINE	9.0	283
E_{e2}	139	0.0	0.5	90	BICINE	9.0	370
E_{e3}	139	0.0	0.5	110	BICINE	9.0	390
F_i	70	20	0.0	0.0	HEPES	7.3	217
F_{e1}	69	0.0	0.5	0.0	HEPES	7.3	119
F_{e2}	69	0.0	0.5	90	HEPES	7.3	228

Solution	Composition (mM)					pH	Osmolality (mOsm/Kg)
	TEACl	EGTA	$CaCl_2{\cdot}2H_2O$	D- Mannitol	Buffer (20 mM)		
F_{e3}	69	0.0	0.5	110	HEPES	7.3	245
G_i	25	20	0.0	0.0	HEPES	7.3	133
G_{e1}	24	0.0	0.5	0.0	HEPES	7.3	64
G_{e2}	24	0.0	0.5	90	HEPES	7.3	139
G_{e3}	24	0.0	0.5	110	HEPES	7.3	162
G_{e4}	24	0.0	0.5	0.0	MES	5.5	67
G_{e5}	24	0.0	0.5	0.0	BICINE	9.0	65
H_i	200	20	0.0	0.0	HEPES	7.3	419
H_{e1}	199	0.0	0.5	0.0	HEPES	7.3	470
H_{e2}	199	0.0	0.5	90	HEPES	7.3	556
H_{e3}	199	0.0	0.5	110	HEPES	7.3	568
I_{e1}	24	0.0	0.5	200	MES	5.5	285±5.0
I_{e2}	24	0.0	0.5	200	HEPES	7.3	287±5.0
I_{e3}	24	0.0	0.5	200	BICINE	9.0	285±5.0
J_i	69	20	0.0	200	HEPES	7.3	361
K_i	25	20	0.0	270	HEPES	7.3	352

Table 2

Parameters used for the kinetic model

Table lists the parameters used for the simulations shown in Fig. 8. Each value was estimated by trial and error.

Parameter	Value or Expression
K_{Cl}	100mM
pK	7
α	2 s^{-1}
β	0.4 s^{-1}
β_v/α_v	20*Exp(-1.0*VF/RT)
f	20

Table 3
Comparison of z and $V_{0.5}$ values obtained from fitting experimental and simulated data

Ionic conditions are indicated in the left column. Statistical differences were evaluated using one way ANOVA with $p<0.5$. z values were statistical different when $[Cl^-]$ decreased from 140 or 70 to 25 mM but not when decreased from 140 to 70 mM. Also z values were different when the pH was varied between 5.5, 7.3 and 9. $V_{0.5}$ values were not different when $[Cl^-]$ was decreased from 140 or 70 to 25 mM but were different by decreasing $[Cl^-]$ from 140 to 70 mM. No statistical differences were found in $V_{0.5}$ when pH was decreased to 5.5 or increased to 9. In contrast $V_{0.5}$ values were different when compared pH 9 and 5.5. Values given are mean±SDM.

	Experiment		Simulation	
Ionic condition	**z**	**$V_{0.5}$ (mV)**	**z**	**$V_{0.5}$ (mV)**
$[Cl]_i$=140, $[Cl]_e$=140, pH=7.3	1.34±0.09	80.8±8.1	1.26	66.9
$[Cl]_i$=70, $[Cl]_e$=140, pH=7.3	1.21±0.14	100.0±10.8	1.24	68.9
$[Cl]_i$=25, $[Cl]_e$=140, pH=7.3	0.76± 0.29	89.8±12.3	1.22	71.5
pH=5.5, $[Cl]_i$=$[Cl]_e$=140	1.33±0.11	63.5±8.	1.37	56.6
pH=7.3, $[Cl]_i$=$[Cl]_e$=140	1.17±0.11	79.3±11.4	1.26	66.9
pH=9, $[Cl]_i$=$[Cl]_e$=140	0.95±0.42	85.1±17.0	1.21	73.3